Journal of Beijing Institute of Technology, 2023, Vol. 32, No. 6

Nonlinear Trajectory SAR Imaging Algorithms: Overview and Experimental Comparison

Yi Xiong, Buge Liang, Ning Wang, Jianlai Chen✉

Abstract: The nonlinear characteristics of the motion trajectory of the synthetic aperture radar (SAR) flight platform can lead to severe two-dimensional space-variance characteristics of the signal, greatly affecting the imaging quality, and are currently considered as one of the difficulties in the field of SAR imaging. This paper first discusses the nonlinear trajectory SAR model and its space-variance characteristics and then discusses algorithms such as scaling-based algorithms, interpolation-based algorithms, time-domain algorithms, and hybrid algorithms. The relative merits and applicability of each algorithm are analyzed. Finally, computer simulation and actual data validation are conducted.

Keywords: two-dimensional space-variance; nonlinear synthetic aperture radar (NL-SAR); slant range model

1 Introduction

Compared to traditional imaging methods, synthetic aperture radar (SAR) imaging technology has stronger environmental adaptability and initiative and can achieve high-precision imaging of target areas in various adverse weather environments by actively emitting electromagnetic waves [1, 2]. The initial synthetic aperture radar was mounted on an aircraft, and the aircraft's motion was planned as an ideal uniform linear trajectory, making it easier for the radar system to implement. Moreover, existing classic frequency domain and beam domain imaging algorithms can be directly used for subsequent imaging processing. However, during actual flight, the flight platform may not strictly follow a linear trajectory due to its own mobility requirements and atmospheric turbulence. Compared to linear monostatic trajectory SAR, nonlinear trajectory SAR has richer target information, stronger flexibility, and maneuverability, and will be one of the important research directions for the future development of SAR technology [3].

The platforms of nonlinear synthetic aperture radar (NL-SAR) include high-resolution medium/high orbit satellite SAR [4–6], ultra-high resolution low orbit satellite SAR [7–10], missile-borne SAR [11, 12], and high mobility platform SAR. The common difficulties faced by different NL-SAR platforms in imaging are: 1) the failure of traditional slant range models; and 2) The radar echo exhibits two-dimensional space-variance characteristics. An accurate echo slant range model is the foundation of subsequent focusing imaging algorithms, while traditional single basis linear trajectory SAR slant range models are difficult to directly apply to nonlinear trajectory SAR, resulting in model mismatch issues. In addition, when the trajectory is

Manuscript received Oct. 27, 2023; revised Dec. 8, 2023; accepted Dec. 18, 2023. The associate editor coordinating the review of this manuscript was Zhiyang Chen. This work was supported in part by the National Natural Science Foundation of China (No. 62271510), in part by Young Elite Scientists Sponsorship Program by CAST (No. 2022QNRC001), in part by the Natural Science Foundation of Hunan Province (No. 2021JJ40781), and in part by the Open Fund of Laboratory of Pinghu.

Yi Xiong, Buge Liang and Jianlai Chen are with School of Automation, Central South University, Changsha 410083, China.

Ning Wang is with Laboratory of Pinghu, Shenzhen 518100, China.

✉ Corresponding author. Email: jianlaichen@163.com

DOI: 10.15918/j.jbit1004-0579.2023.106

planned to be nonlinear, the radar echo not only has range space-variance but also has azimuth space-variance. The traditional frequency domain algorithm based on the assumption of azimuth translation invariance cannot be directly used to process two-dimensional space-variance signals.

In summary, high-precision NL-SAR slant range models and algorithms will be the difficulty and key direction of future research. Innovative new imaging algorithms will be the goal of every researcher. This article first introduces the existing NL-SAR slant range models and then focuses on elaborating on several types of processing algorithms. The advantages and disadvantages of each type of algorithm are discussed. Finally, simulation and measured data are used to verify, and prospects and suggestions for future NL-SAR imaging are provided.

2 NL-SAR Echo Model

2.1 Slant Range Model

From a kinematic perspective, the slant range model mainly describes the relative motion between the radar platform and the observed target, and an accurate slant range model is the foundation for subsequent imaging. Traditional ideal linear trajectory SAR platforms and low orbit spaceborne SAR platforms with short-term observations can accurately describe their motion state using classic hyperbolic slant range models, shown as

$$R(t_a)=\sqrt{r^2+(v(t_a-t_0))^2} \tag{1}$$

where t_a denotes the azimuth time, r denotes the shortest slant range, t_0 is the zero-Doppler time, v denotes the equivalent velocity. For the slant range signal model in Eq. (1), precise imaging can be achieved using traditional frequency domain imaging algorithms. However, in the actual flight process, the flight platform may be affected by factors such as ground terrain and atmospheric turbulence, as well as its own maneuverability requirements, which may not strictly follow a straight trajectory. In the case of nonlinear trajectories, the slant range error of the hyperbolic function is relatively large, making it unsuitable for NL-SAR imaging.

The model of NL-SAR is shown in Fig. 1. Regarding the motion characteristics of airborne NL-SAR, the nonlinear trajectory slant range can be expressed as the sum of linear parts and errors [13], as follows

$$R(t_a)=\sqrt{r^2+(v(t_a-t_0))^2}+\Delta R(t_a) \tag{2}$$

where $\Delta R(t_a)$ is the deviation slant range from the orbit. In general, it is difficult to obtain the analytical expression of $\Delta R(t_a)$, which is not conducive to subsequent imaging processing. A non space-variance motion error compensation model based on Eq. (2) is proposed by [14], which only considers the non space-variance characteristic of $\Delta R(t_a)$ and ignores its two-dimensional space-variance. With the improvement of resolution and the width of the mapping strip, the impact of the space-variance characteristic on imaging will become more significant. Therefore, this model is not suitable for situations with wide mapping bands and high resolution. On this basis, a two-dimensional space-variance motion error slant range model is proposed in [15], which takes into account the two-dimensional space-variance characteristics of $\Delta R(t_a)$ and considers $\Delta R(t_a)$ as composed of azimuth space-variance motion error, range space-variance motion error, coupling term motion error, and non space-variance motion error. Through the correction of two-dimensional space-variance

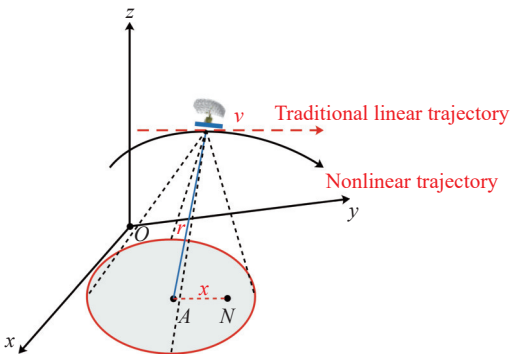

Fig. 1 Geometry of NL-SAR

error, high-resolution imaging of large swaths can be achieved.

Unlike airborne SAR, the nonlinear trajectory of spaceborne SAR is caused by the satellite platform's orbit around the Earth. Therefore, for spaceborne SAR, observation time and orbit height will have an impact on the degree of curvature of the satellite trajectory. In [16], the original slant range model is proposed, although this model can accurately represent the oblique slant range, it does not have an analytical expression, which is not conducive to subsequent imaging processing. The high-order polynomial model is currently widely used in airborne /spaceborne SAR data processing [17]. This model approximates the slant range into a high-order polynomial form regarding azimuth time. The higher the order, the higher the accuracy, and the higher the complexity of subsequent processing. In [8], a motion compensation principle slant range model is proposed from the perspective of motion compensation, which decomposes the slant range of the target into hyperbolic slant range and error slant range introduced by trajectory offset. By adjusting the accuracy of the error slant range, the slant range of the target can be accurately expressed. This model does not require strict imaging geometric correspondence and is more flexible in application scenarios. An equivalent acceleration model is proposed in [18] for spaceborne SAR, which is mainly based on the hyperbolic slant range model and corrects the space-variance of equivalent velocity by adding equivalent acceleration and error function. This model can accurately process spaceborne SAR data in large azimuth mapping zones and ultra-high resolution situations.

2.2 Analysis of the Space-Variance

For traditional linear trajectory SAR (L-SAR), the range cell migration (RCM) trajectory curvature of targets at different azimuth positions is consistent, and imaging can be achieved by using traditional frequency domain algorithms to correct for range variability. However, for NL-SAR, due to the nonlinearity of the motion trajectory, the trajectory curvature of the point target RCM located at different azimuth positions is inconsistent (as shown in Fig. 2), which cannot be corrected through a unified matched filtering function and results in azimuth space-variance. Therefore, traditional frequency domain algorithms based on the assumption of azimuth translation invariance are not suitable for NL-SAR imaging. For NL-SAR imaging, the most crucial issue is how to correct azimuth space-variance.

3 Review of Scaling-Based Algorithms

The scaling-based algorithm is based on the scaling principle proposed by Papoulis. This type of algorithm corrects the signal characteristics of all targets in the imaging area to be consistent with the reference point target through the scaling (see Fig. 3), completing the correction of signal

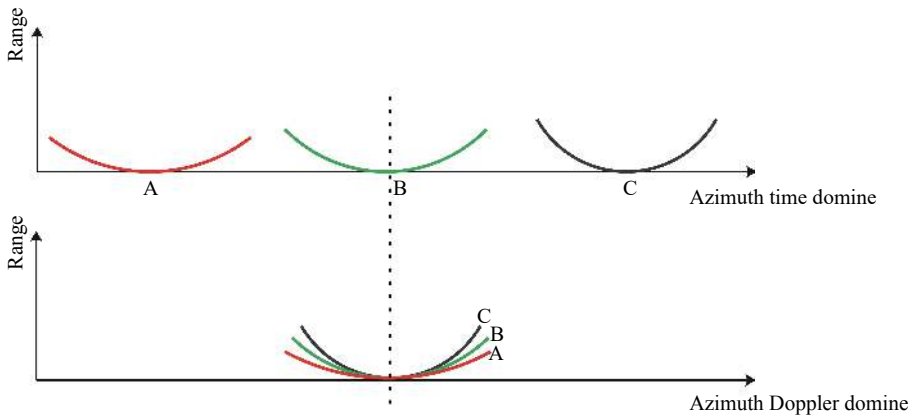

Fig. 2 Schematic diagram of azimuth space-variance

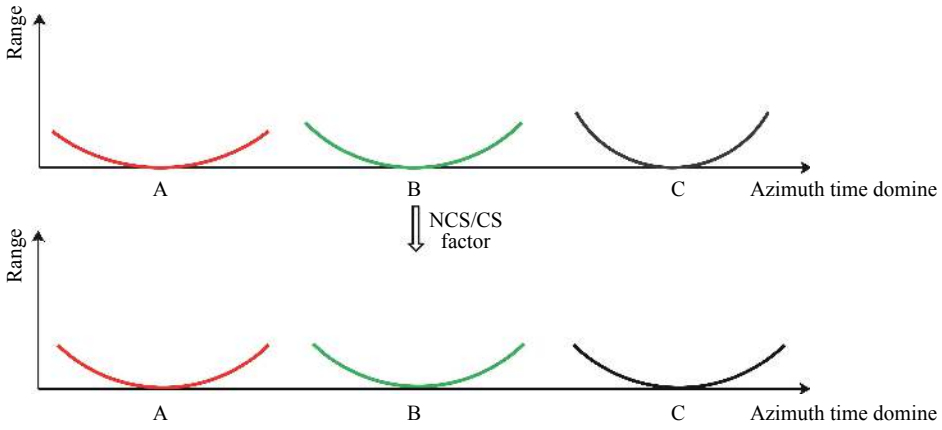

Fig. 3 Schematic diagram of CS/NCS

space-variance characteristics. At present, this type of algorithm mainly includes chirp scaling algorithm (CSA), frequency scaling algorithm (FSA), nonlinear CSA (NCSA) and its extension algorithms.

CSA, as the earliest scaling-based algorithm, is widely used in airborne imaging and is currently a relatively mature algorithm [19]. Subsequently, scholars have proposed an extension form of the CSA algorithm to meet the needs of large squint under certain conditions [20]. The imaging principle of the FSA is the same as that of CSA, which corrects the range migration and azimuth Doppler parameters of spatial variability through scaling. However, when the trajectory is nonlinear, complex motion states can lead to severe coupling and two-dimensional space-variance characteristics of the signal, and using CSA or FSA can result in significant approximation errors. Therefore, for NL-SAR imaging, we generally use higher-order NCS algorithms. At present, many scholars have proposed the NCS algorithm and its extension algorithm for NL-SAR imaging, which have been applied on multiple platforms such as airborne, spaceborne, and missile-borne platforms, greatly expanding the scope of use of scaling-based algorithms.

For airborne SAR imaging, most of the existing NCS algorithms are based on linear trajectories or simple two-dimensional space-variance configurations of bistatic SAR, without considering the case of nonlinear trajectories and three-dimensional acceleration. Therefore, there is still room for research and development in the application of NCS in airborne nonlinear trajectory SAR imaging. An extended azimuth NCS (ANCS) algorithm is proposed in [21] for arbitrary trajectory models with three-dimensional acceleration. By utilizing the nonlinear relationship between target position and azimuth frequency, a multiphase filter is combined with a variable standard to improve the degree of freedom of the variable standard and effectively remove the azimuth spatial variation characteristics. In [22], a two-step NCS algorithm based on sub-aperture blocking is proposed for nonlinear trajectory bistatic SAR. The first step uses a 4th-order scaling function to correct the 3rd order space-variance term, and the second step combines the sub-aperture blocking strategy with the 3rd-order NCS to correct the 2nd-order space-variance term to achieve azimuth unified focusing. However, blocking may increase the complexity of the algorithm and may also lead to positional offset.

For spaceborne SAR imaging, the NCS algorithm has a wide range of applications in low-orbit and medium/high-orbit imaging. In [23], the NCS algorithm is proposed for mid-orbit spaceborne SAR, further improving the width of the mapping band. In [24], a range block strategy is used to correct for distance spatial variation, and then NCS to correct the remaining azimuth spatial variation. However, the number

of blocks may affect the efficiency and accuracy of the algorithm. In [25], a two-dimensional NCS algorithm is proposed, which uses NCS for space-variance correction in both range and azimuth, effectively improving the width of the range mapping strip and the focusing quality in azimuth. In the future development of spaceborne SAR imaging, the innovative application of the NCS algorithm will be one of the key research directions.

It is also worth noting that in order to achieve monitoring and imaging of scenes outside the region, SAR often operates in squint mode. In the case of squint mode, the echo will exhibit a first-order coupling of distance and azimuth, making RCM exceptionally complex. An NCS algorithm is proposed in [26], which only considers the spatial variability of the secondary range compression (SRC) term, but does not analyze the spatial variability of higher-order terms. Therefore, this algorithm is only applicable to situations with low squint mode. In [27, 28], an azimuth nonlinear chirp scaling algorithm is proposed for highly squint SAR, which introduces azimuth NCS function to correct the azimuth space-variance of azimuth frequency modulation ratio. As the resolution improves and the mapping zone expands, the quadratic range cell migration (QRCM) azimuth space-variance becomes more and more obvious, and the defocusing of scene edge points will also become more severe. In response to this issue, An improved NCS algorithm is proposed in [29], which considers both phase and QRCM azimuth space-variance. It performs range NCS processing to correct RCM on the signal before range pulse compression and QRCM correction. However, there are multiple approximations in the algorithm derivation process and the processing is relatively complex.

Most existing NCS algorithms are below 4th order. Considering generality, the NCS function can theoretically be expressed as an nth-order polynomial

$$\varphi_{\mathrm{NCS}}(t_a) = \alpha_1 t_a^3 + \alpha_2 t_a^4 + \cdots + \alpha_{n-2} t_a^n \tag{3}$$

where α is the coefficient of the polynomial. To further illustrate the role of NCS in correcting RCM azimuth space-variance, referring to [22], $\Delta R(t_a)$ in Eq. (2) can be modeled as follows

$$\Delta R(t_a) \approx a_0 (t_a - t_0)^2 + b_0 (t_a - t_0)^3 \tag{4}$$

where a_0 and b_0 are the coefficients of quadratic and cubic errors, respectively, and can be modeled as first-order space-variance expressions about t_0, namely

$$a_0 = a_{00} + a_{01} t_0 \tag{5}$$

$$b_0 = b_{00} + b_{01} t_0 \tag{6}$$

From Eq. (4), it can be seen that the approximation error function has two-dimensional space-variance and cannot be corrected by a unified matched filter function. Therefore, it is necessary to introduce a higher-order scaling function for scaling processing. Firstly, a third-order polynomial NCS function is introduced

$$H_{3\mathrm{rd}}(t_a) = \exp\left(-\mathrm{j}\frac{2\pi}{\lambda}\alpha_1 {t_a}^3\right) \tag{7}$$

when $\alpha_1 = -a_{01}/3$, the cubic scaling function can effectively correct the first-order azimuth space-variance of quadratic error, while also introducing second-order space-variance of primary error, The detailed derivation process can refer to [22]. For the remaining cubic space-variance error, pure third-order NCS functions cannot be corrected, and the fourth-order scaling function in following equation needs to be introduced

$$H_{4\mathrm{th}}(t_a) = \exp\left(-\mathrm{j}\frac{2\pi}{\lambda}\beta {t_a}^4\right) \tag{8}$$

Referring to [22], it can be seen that when $\beta = -b_{01}/4$, the quartic scaling function can effectively correct the first-order azimuth space-variance characteristics of the cubic error, but it also introduces additional space-variance terms. The newly introduced null variable term will seriously affect the focusing quality of the image, resulting in inconsistent focusing quality between the left and right scenes.

In summary, NCS is an effective method for correcting the azimuth space-variance characteristics of signals. It only requires simple calibration processing and time-frequency conversion to complete imaging, with high imaging efficiency. Generally speaking, the higher the order of the scaling function, the better its focusing effect. However, the complexity of solving the NCS function will also increase, and additional space-variance terms will be introduced, which will affect the quality of imaging and the position of focus. Therefore, the order of the NCS function generally does not exceed 4 orders. However, with the complexity of the oblique motion model and motion characteristics of the NL-SAR platform, especially in the presence of three-dimensional acceleration, high squint, and other situations, there may be space-variance errors of high order. Traditional 4th order and lower order NCS have difficult to meet the requirements of high-precision imaging, so this method may be applicable to NL-SAR configurations with relatively simple space-variance characteristics.

4 Review of Interpolation-Based Algorithms

The basic idea of interpolation-based algorithms is to find accurate interpolation kernels and perform interpolation processing on the signal to achieve signal space-variance correction. Traditional interpolation algorithms such as RMA can only correct one-dimensional range space-variant signals and are not suitable for NL-SAR imaging. Therefore, the main problem of using interpolation algorithms to correct NL-SAR space-variance characteristics is to solve the interpolation kernel in the azimuth direction. Currently, the methods of azimuth interpolation can be classified into two categories: frequency domain interpolation and time domain interpolation.

4.1 Frequency Domain Interpolation Algorithm

Frequency domain interpolation is the most common form of interpolation algorithms, mainly by approximating the azimuth space-variance term in the two-dimensional spectrum as first-order terms of azimuth position information based on the obtained two-dimensional spectrum, and then obtaining the azimuth interpolation kernel. The methods for solving interpolation kernels mainly include formula derivation, singular value decomposition (SVD), etc.

4.1.1 Frequency Domain Interpolation Algorithm Based on Formula Derivation

The frequency domain interpolation algorithm based on formula derivation is mainly based on the obtained two-dimensional spectrum, combined with the signal model to derive a new azimuth interpolation kernel. Unlike linear trajectory SAR, NL-SAR cannot directly solve the two-dimensional spectrum using the stationary phase method. The method of series reversion (MSR) is currently the most commonly used method for solving the two-dimensional spectrum of NL-SAR signals. After MSR, the two-dimensional spectrum of NL-SAR can be represented as

$$\begin{aligned}\varphi(f_a,x)=&-2\pi\Big(k_0+t_0(f_a+k_1)-\\&\frac{1}{4k_2}(f_a+k_1)^2-\frac{k_3}{8{k_2}^3}(f_a+k_1)^3-\\&\frac{(9{k_3}^2-4k_2k_4)}{64{k_2}^5}(f_a+k_1)^4\Big)\end{aligned}\tag{9}$$

where $k_i(x)$ is the coefficient related to azimuth position, and the above formula ignores range information. When the motion state and parameters of the radar are determined, the value of $k_i(x)$ is known. To simplify Eq. (9), we can approximately model it as a first-order spatiotemporal model with respect to the azimuth position, i.e. $k_1\approx\sigma-\beta t_0$. The two-dimensional spectrum of the signal can be organized into

$$\begin{aligned}\varphi(f_a,x)\approx&-2\pi(\phi_0+(\phi_{10}+\phi_{11}t_0)f_a+\\&(\phi_{20}+\phi_{21}t_0){f_a}^2+(\phi_{30}+\phi_{31}t_0){f_a}^3+\\&(\phi_{40}+\phi_{41}t_0){f_a}^4)\end{aligned}\tag{10}$$

where $\phi_i\approx\phi_{i0}+\phi_{i1}t_0(i=1,2,3,4)$ is the coeffi-

cient of ith order space-variance.The above formula can be organized as

$$\varphi(f_a,x)\approx -2\pi(\phi_0+\phi_{10}f_a+\phi_{20}{f_a}^2+\phi_{30}{f_a}^3+\phi_{40}{f_a}^4+\phi_{11}t_0(f_a+\beta_1{f_a}^2+\beta_2{f_a}^3+\beta_3{f_a}^4)) \tag{11}$$

where

$$\begin{cases}\beta_1=\dfrac{\phi_{21}}{\phi_{11}}\\ \beta_2=\dfrac{\phi_{31}}{\phi_{11}}\\ \beta_3=\dfrac{\phi_{41}}{\phi_{11}}\end{cases} \tag{12}$$

The azimuth interpolation kernel can be expressed as

$$f_a'=f_a+\beta_1{f_a}^2+\beta_2{f_a}^3+\beta_3{f_a}^4 \tag{13}$$

The values of β_1, β_2, and β_3 in Eq. (12) are generally implicit functions related to the radar motion state and radar parameters. Interpolation algorithms based on formulas mainly use existing mathematical tools and approximate processing to solve the analytical explicit expression of $\{\beta_1,\beta_2,\beta_3\}$, and the obtained analytical expression can be used to correct the azimuth spatial variation characteristics of the signal through interpolation. A generalized $\omega-k$ algorithm is proposed in [30] for azimuth space-variance bistatic SAR, which obtains a two-dimensional spectrum through generalized Loffeld's bistatic formula (GLBF). Then, a new two-dimensional interpolation is derived to correct azimuth space-variance, transforming the signal from the frequency domain to the time domain to complete the final imaging. In [21], a two-dimensional keystone algorithm is proposed in the azimuth frequency domain for curve trajectories. This algorithm uses two-dimensional Taylor series expansion to obtain the linear relationship descriptions of the first-order and second-order expressions in the azimuth frequency domain. Based on this description, the two-dimensional signal is redistributed to obtain a two-dimensional interpolation kernel, which is then subjected to two-dimensional interpolation processing.

Overall, the core of frequency domain interpolation algorithms based on formula derivation lies in how to linearize the two-dimensional spectrum with respect to distance and azimuth positions based on the existing two-dimensional spectrum. Only the linearized phase can perform uniform interpolation processing on the non-uniform two-dimensional spectrum, otherwise, it is difficult to achieve precise focused imaging processing of the scene using IFFT. It is also worth noting that approximation processing may be used during the derivation process, so such algorithms may be difficult to adapt to complex flight environments.

4.1.2 Frequency Domain Interpolation Algorithm Based on SVD

As the complexity of the motion characteristics of radar flight platforms increases, the coupling characteristics of azimuth position and azimuth frequency will become more severe, and the accuracy of methods derived through formulas may not meet the imaging requirements. SVD, as a mathematical tool, can be used to separate the coupling characteristics of signals. It can be used for both distance spatially variable phase decomposition and azimuth spatially variable phase decomposition. Generally speaking, after SVD, two feature vectors can fully represent the signal, and the decomposition process can be expressed as

$$\phi_a(f_a;R_b,X)=u_{a1}(R_b,X)s_{a1}v_{a1}(f_a,R_b)+u_{a2}(R_b,X)s_{a2}v_{a2}(f_a,R_b) \tag{14}$$

$$\phi_r(f_r,f_a;R_b)=u_{r1}(R_b,f_a)s_{r1}v_{r1}(f_r,f_a)+u_{r2}(R_b,f_a)s_{r2}v_{r2}(f_r,f_a) \tag{15}$$

where $\phi_a(f_a;R_b,X)$ is azimuth signal,$\phi_r(f_r;f_a,R_b)$ is range signal. SVD-STOLT algorithm is proposed in [31] based on the decomposition principle of SVD, which directly uses the first feature component to interpolate and correct the azimuth space-variance characteristics of the signal. However, in complex environments, the space-variance characteristics of signals may

require two feature vectors to fully represent them, and interpolation using only one feature component can cause significant errors and affect imaging quality. A two-dimensional SVD algorithm is proposed in [32] for spaceborne SAR, which first uses optimal linear range walk correction (LRWC) to reduce azimuth space-variance, and then uses two-dimensional SVD interpolation to correct range space-variance and remaining azimuth space-variance, respectively. It is worth noting that the algorithm introduces a range-blocking strategy in range SVD, which effectively reduces the errors that may be caused by SVD. In azimuth SVD, the azimuth signal is expressed as the sum of two feature vectors, and then the tandem SVD (TSVD) is used to complete focusing imaging. In [3], a controlled SVD (CSVD) algorithm is proposed. This algorithm decomposes the signal into a representation of the sum of feature components through SVD and then obtains a new interpolation kernel through integration operations. Finally, the new interpolation kernel is interpolated to correct the space-variance characteristics of the signal.

In general, obtaining interpolation kernels through SVD is currently a highly accurate method and has broad application prospects in practical imaging environments.

4.2 Time Domain Interpolation Algorithm

Generally speaking, the accuracy of frequency domain interpolation algorithm is closely related to the accuracy of the two-dimensional spectrum of NL-SAR signals. However, as the complexity of the NL-SAR diagonal model increases, the accuracy of the two-dimensional spectrum obtained through method of series reversion (MSR) or Loffeld's bistatic formula (LBF) is difficult to guarantee, and frequency domain interpolation is difficult to meet real-time requirements.

In recent years, scholars have continuously studied the problem of time-domain interpolation imaging. A real-time imaging algorithm with variable pulse repetition frequency (PRF) is proposed in [33], which essentially resamples the sampling time of the transmitted signal and corrects the azimuth space-variance characteristics of the signal during the transmission stage, effectively improving the real-time performance of the algorithm. A spaceborne SAR imaging algorithm based on time-frequency joint resampling is proposed in [34]. This algorithm first corrects the quadratic azimuth space-variance term through time-domain resampling, then corrects the range space-variance term through the algorithm CSA, and finally achieves focused imaging by correcting the remaining high-order azimuth space-variance term through frequency-domain resampling.

There is currently limited research on time-domain interpolation algorithms, and their main application is to interpolate the azimuth time during the signal transmission stage, which has important application prospects in NL-SAR real-time imaging research.

5 Hybrid Algorithm for Interpolation and Scaling

In complex NL-SAR imaging environments, single scaling or interpolation algorithms have their own inevitable drawbacks. Currently, advanced NL-SAR imaging algorithms often combine the two types of algorithms in series to achieve efficient and high-precision imaging. keystone transform and frequency NCS are used to complete the focusing imaging of NL-SAR in [35]. Firstly, an improved second-order keystone transform is used to complete RCMC, and then the frequency scaling function is used to correct the azimuth space-variance. A medium to high orbit SAR imaging algorithm based on the principle of optimal imaging coordinate system is proposed in [36]. This algorithm introduces linear and quadratic terms in the time domain to solve the problem of Doppler frequency modulation linear and nonlinear azimuth space-variance. Then, the NCS algorithm is used to correct the range

space-variance of RCM, and finally, the remaining high-order azimuth space-variance terms are corrected using frequency domain resampling.

The combination of scaling-based and interpolation-based algorithms will leverage their respective advantages throughout the entire imaging process, effectively improving the accuracy and efficiency of imaging, making it a hot topic and direction for future research on high-resolution NL-SAR imaging.

6 Time Domain Algorithm

Compared with frequency domain imaging algorithms, the time-domain algorithm relies on accurate calculation of instantaneous slope distance, and there is no decoupling process of echo signals. Essentially It is suitable for any radar platform trajectory, any imaging mode system, and can achieve high-precision imaging under high oblique and curved trajectories, making them more adaptable to complex signal models of NL-SAR.

Typical time-domain algorithms mainly include back-projection (BP) [37] and fast back-projection (FBP) [38]. The BP algorithm mainly restores the backscattered energy of the target through precise compensation of range phase and coherent accumulation of azimuth, achieving point-to-point imaging. It does not introduce approximation operations in the derivation process, resulting in good imaging results. However, the computational complexity is large, making it difficult to meet the fast imaging needs of wide scenes [39]. Although the FBP algorithm reduces computational complexity through sub-aperture blocking and other processing, its computational efficiency is still low. In [40], an accelerated FBP (AFBP) is proposed. This algorithm introduces the concept of wavenumber spectrum and achieves aperture fusion through the concatenation of wavenumber spectra, avoiding image interpolation operations and effectively improving imaging efficiency. A Cartesian factorized BP (CFBP) algorithm is proposed in [41, 42], it derives the image spectrum in a Cartesian coordinate system and achieves aperture fusion through spectrum concatenation, directly obtaining Cartesian coordinate images. However, AFBP and CFBP are based on linear trajectories, and further research is needed to determine whether they can be used in NL-SAR.

Overall, processing NL-SAR imaging based on time-domain algorithms is currently the most accurate type of processing algorithm in theory. However, time-domain algorithms perform coherent accumulation imaging point by point, making it difficult to rely on Fourier transform (FT) for fast computation. Therefore, compared to frequency-domain algorithms, time-domain algorithms have higher computational complexity and longer imaging time. Improving time-domain imaging speed requires research from both hardware and software levels: firstly, improving the computational efficiency of digital processors and designing efficient parallel processing architectures; The second is to study fast time-domain imaging algorithms to reduce the computational complexity of time-domain imaging.

7 Verification of Simulation and Measure Data

In this section, we will conduct simulation and measure data validation on scaling-based algorithms and interpolation-based algorithms.

The motion and simulation parameters of the NL-SAR platform are shown in Tab. 1, and the distribution of simulated scene targets is

Tab. 1 Main system parameters

Simulation parameter	Value
Closest slant range	17 500 m
Initial velocity	(49.2, 13.8, 0) m/s
Acceleration	(–0.01, 0.02, 0) m^2/s
Carrier frequency	16 GHz
PRF	1 000 Hz
Signal bandwidth	1 400 MHz
Azimuth resolution	0.1 m

shown in Fig. 4. A set of 5 × 5 targets (azimuth × range) are placed on the ground uniformly with a scene size of 400 m × 270 m (azimuth × range). Target P is the left edge point, target Q is the right edge point. Firstly, we refer to [22] and [35] to obtain the coefficients of the NCS function and interpolation kernel. Then, we use the center point matching filtering algorithm, NCS algorithm, and interpolation-based algorithm for simulation imaging, and select P and Q as evaluation points. The results of matched filtering are shown in Fig. 5, while the results of the NCS algorithm and interpolation-based algorithm are shown in Figs. 6–9. In addition, the quantitative evaluation results are shown in Tab. 2, including the azimuth PSLR and the azimuth ISLR.

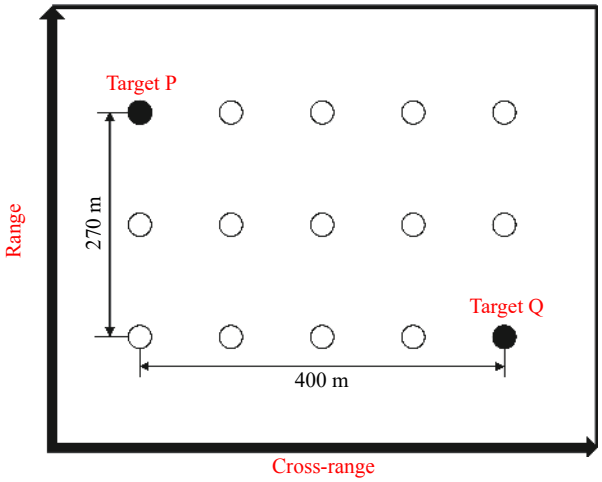

Fig. 4 Scene of 300 m (azimuth) × 200 m (range) (15 targets are evenly distributed in the scene)

Fig. 5 shows that the signal still exhibits severe defocusing after matched filtering. From Figs. 6 (a) and 8 (a), it can be seen that the third-order NCS can effectively correct the second-order space-variance of the signal, but cannot correct the third-order space-variance, resulting in sidelobe asymmetry. From Fig. 6 (b), it

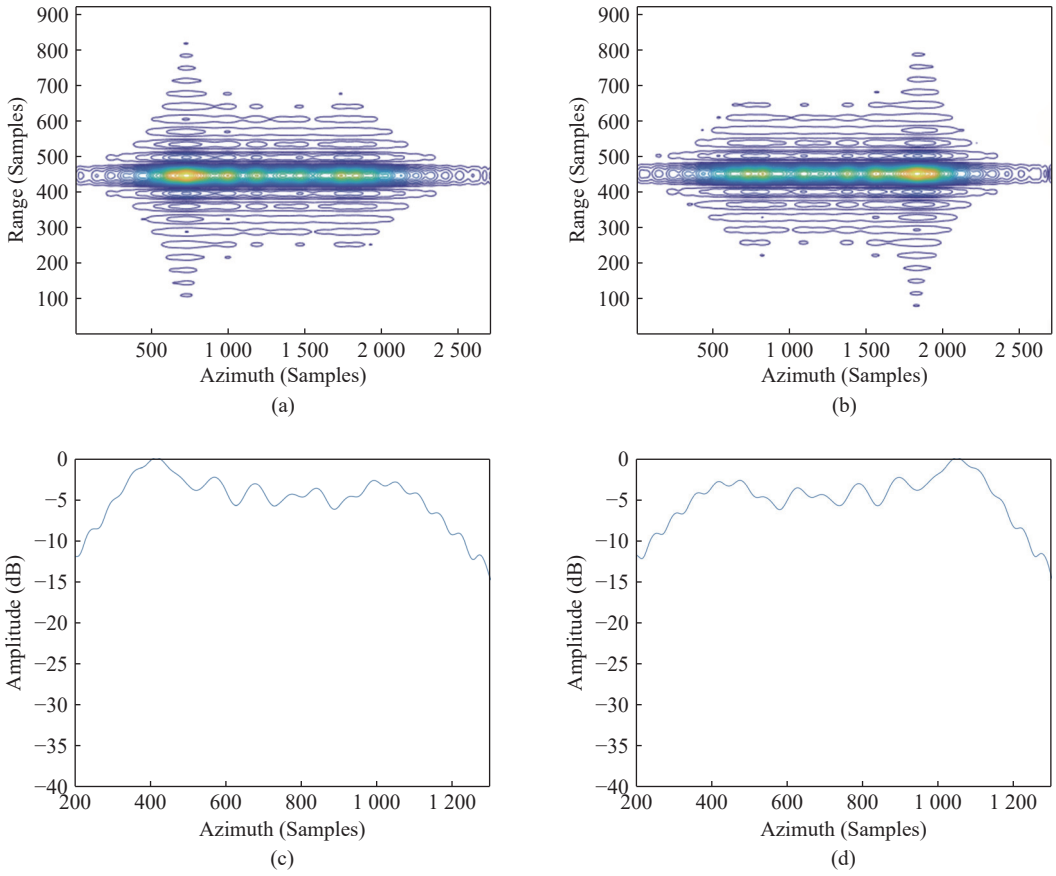

Fig. 5 Results of matched filtering: (a) contours of the target P; (b) contours of the target Q; (c) azimuth profile of the target P; (d) azimuth profile of the target Q

can be seen that after adding a fourth-order NCS, the third-order space-variance of point target P has been effectively corrected, and the focusing quality of point target P has been greatly improved. However, from Fig. 8 (b), it can be seen that the imaging quality of point target Q has not been effectively improved after adding a fourth-order NCS. This is mainly due to the additional space-variance introduced by NCS, which results in inconsistent focusing quality on the left and right sides of the scene. From Figs. 6 (c) and 8 (c), it can be seen that second-order RS can effectively correct the second-order space-variance of the signal, but cannot correct the third-order space-variance, resulting in sidelobe asymmetry. From Figs. 6 (d) and 8 (d), it can be seen that the third-order space-variance of the two edge points has been effectively corrected after adding the third-order RS. Meanwhile, the quality parameters in Tab. 2 also validate the above conclusion.

Tab. 2 Imaging evaluation results of selected targets

Algorithm	Target	Azimuth PSLR (dB)	Azimuth ISLR (dB)
Match filter	Target P	–2.23	–5.16
	Target Q	–2.24	–5.17
2-order NCS	Target P	–6.43	–7.74
	Target Q	–6.45	–7.89
'2+3'-order NCS	Target P	–13.02	–9.76
	Target Q	–8.02	–8.10
2-order RS	Target P	–6.65	–7.80
	Target Q	–6.71	–7.91
'2+3'-order RS	Target P	–13.04	–9.82
	Target Q	–13.10	–9.85

Next, we will use measured data for verification. The radar platform operates in the Ku band, with a speed of approximately 48.6 m/s and a bandwidth of 1.4 GHz. The synthetic aperture time is approximately 25 s, and the PRF is 1 000 MHz. It should be noted that the motion errors in the measured data are usually unknown, so we need to use the estimation methods in [22]

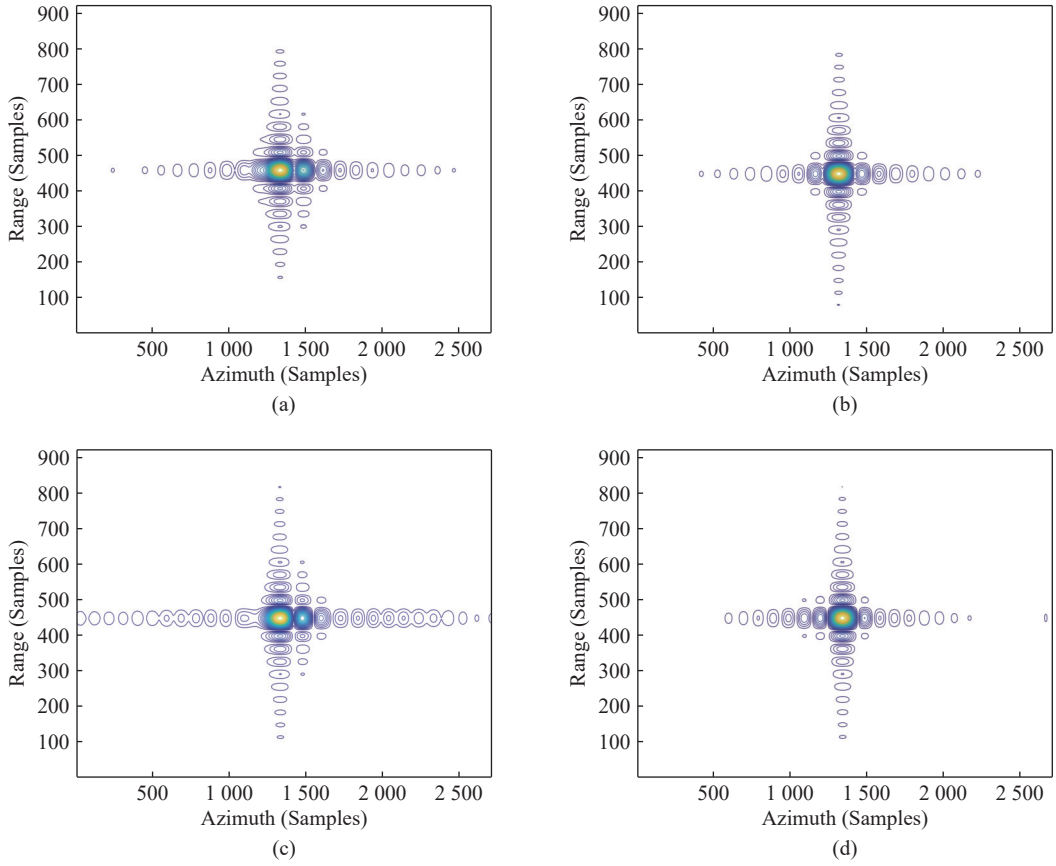

Fig. 6 Contours of the target P by using: (a) 3-order NCS; (b) '3+4'-order NCS; (c) 2-order RS; (d) '2+3'-order RS

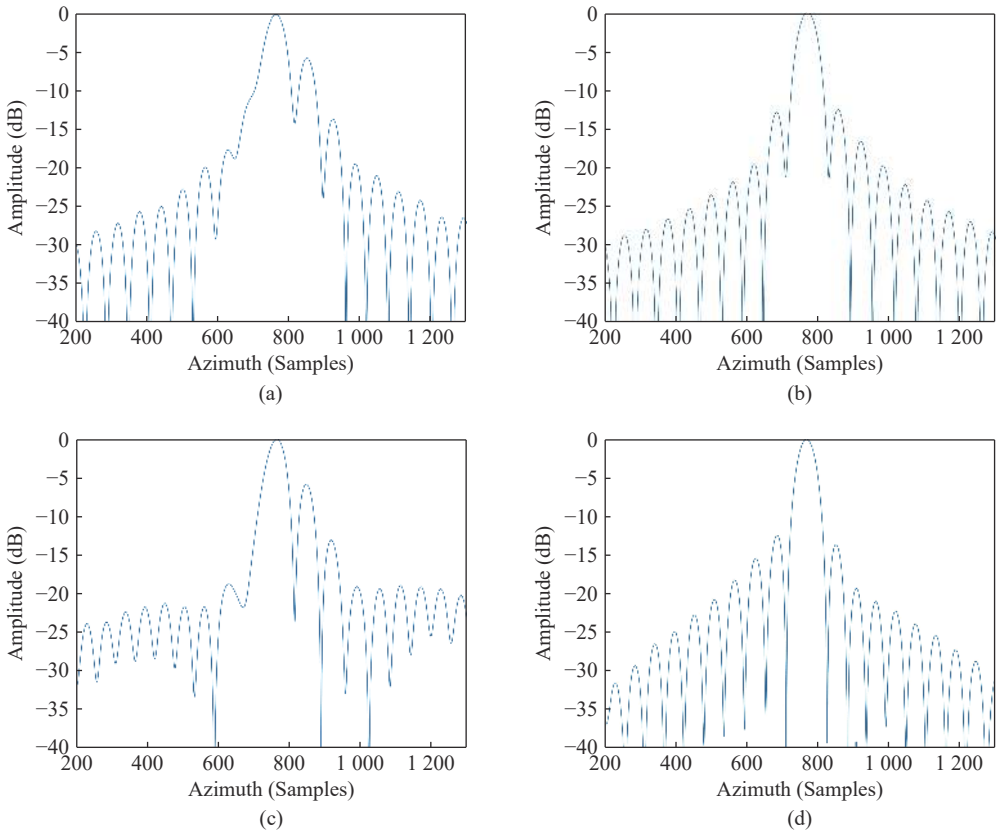

Fig. 7 Azimuth profiles of the target P by using: (a) 3-order NCS; (b) '3+4'-order NCS; (c) 2-order RS; (d) '2+3'-order RS

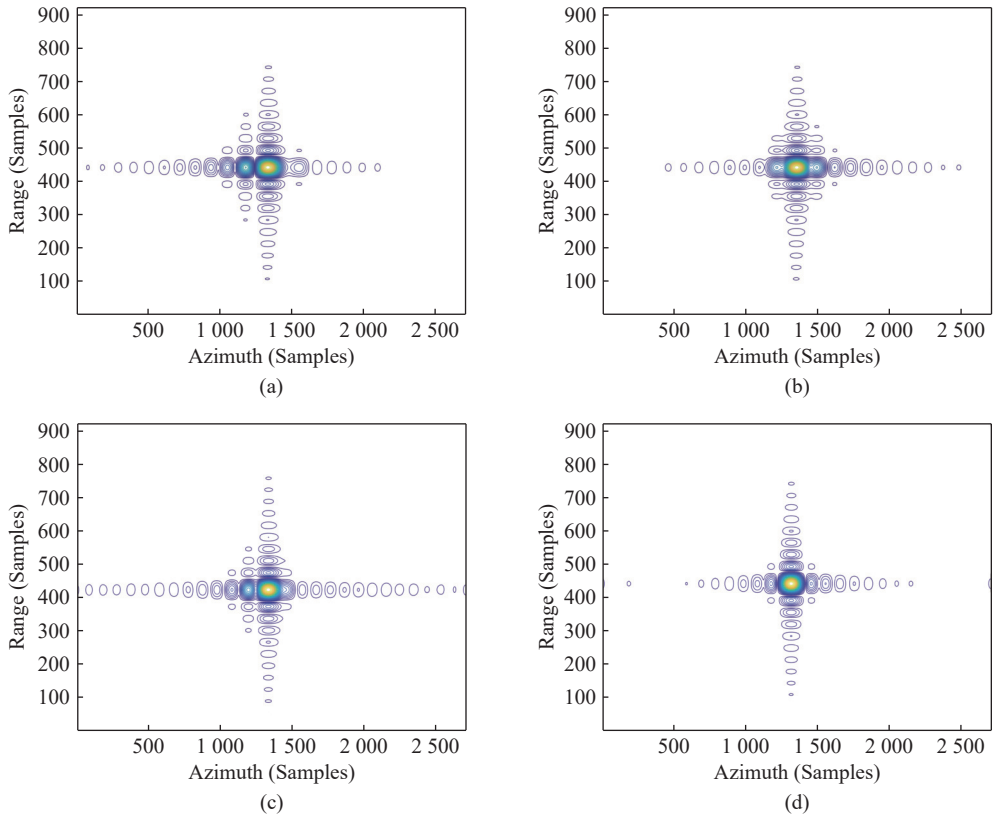

Fig. 8 Contours of the target Q by using: (a) 3-order NCS; (b) '3+4'-order NCS; (c) 2-order RS; (d) '2+3'-order RS

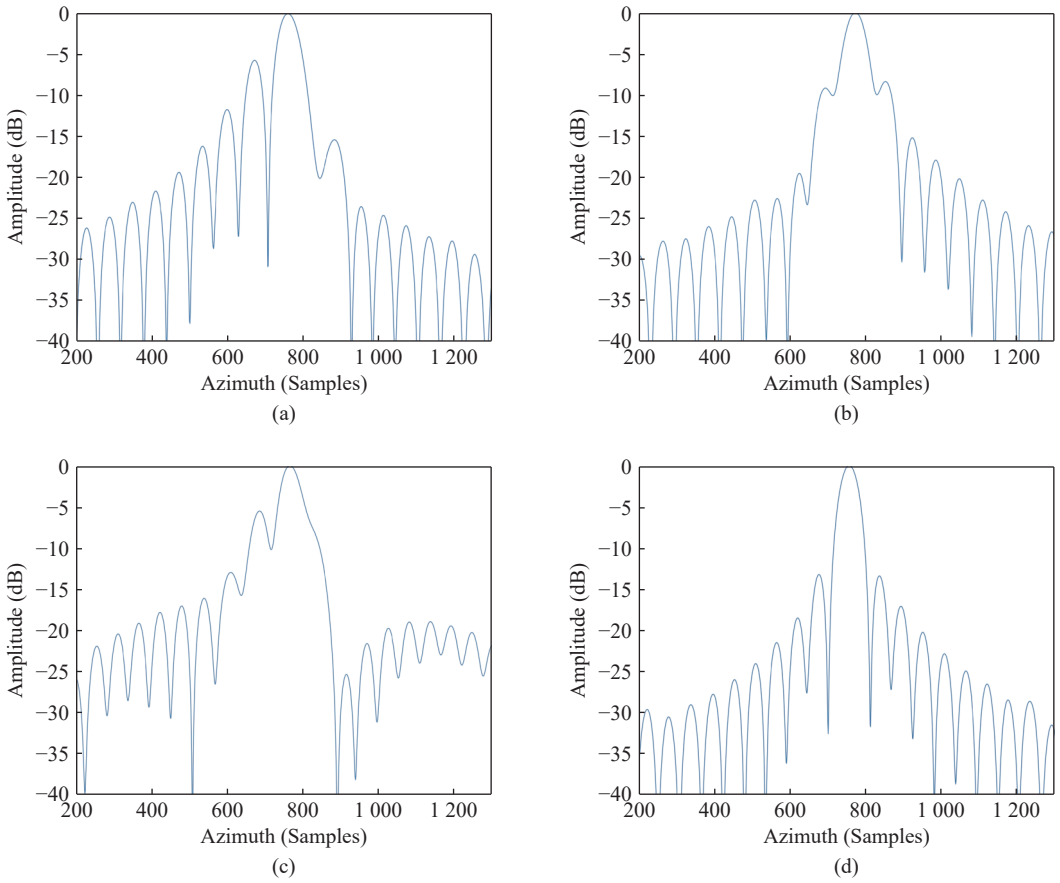

Fig. 9 Azimuth profiles of the target Q by using: (a) 3-order NCS; (b) '3+4'-order NCS; (c) 2-order RS; (d) '2+3'-order RS

and [39] to obtain the relevant nonlinear scaling function and interpolation kernel. Then, the measured data are processed using two-step, 3-order NCS, '3+4'-order NCS, 2-order RS, and '2+3'-order RS respectively, and the results are shown in Fig. 10. From Fig. 10 (a), it can be seen that the long synthetic aperture time leads to severe azimuth space-variance in the signal, and the traditional two-step algorithm has poor imaging quality. However, using pure third-order NCS or second-order RS can only correct the second-order space-variance characteristics, and the higher-order term of space-variance still exists, so the image still has defocusing (as shown in Figs. 10 (b) and (d)). After introducing a 4th-order NCS on top of the 3rd-order NCS (as shown in Fig. 10 (c)), the imaging quality of the right end scene is further improved, while the left end is not significantly improved. After introducing third-order RS on top of second-order RS (as shown in Fig. 10 (e)), the imaging quality at both ends of the scene has been improved. However, it is worth mentioning that interpolation operation can bring a certain degree of computational complexity, so imaging efficiency also needs to be considered. In order to better evaluate image quality, we use image entropy to evaluate the imaging results of each algorithm. The evaluation results are shown in Tab. 3. The smaller the entropy value, the better the image quality. Obviously, '2+3'-order RS is superior.

Tab. 3 Entropy evaluation results of local enlarged images in Fig. 10

Algorithm	Left end area	Right end area
Match filter	11.168	10.685
2-order NCS	11.015	10.476
'2+3'-order NCS	10.998	10.471
2-order RS	11.016	10.475
'2+3'-order RS	10.995	10.468

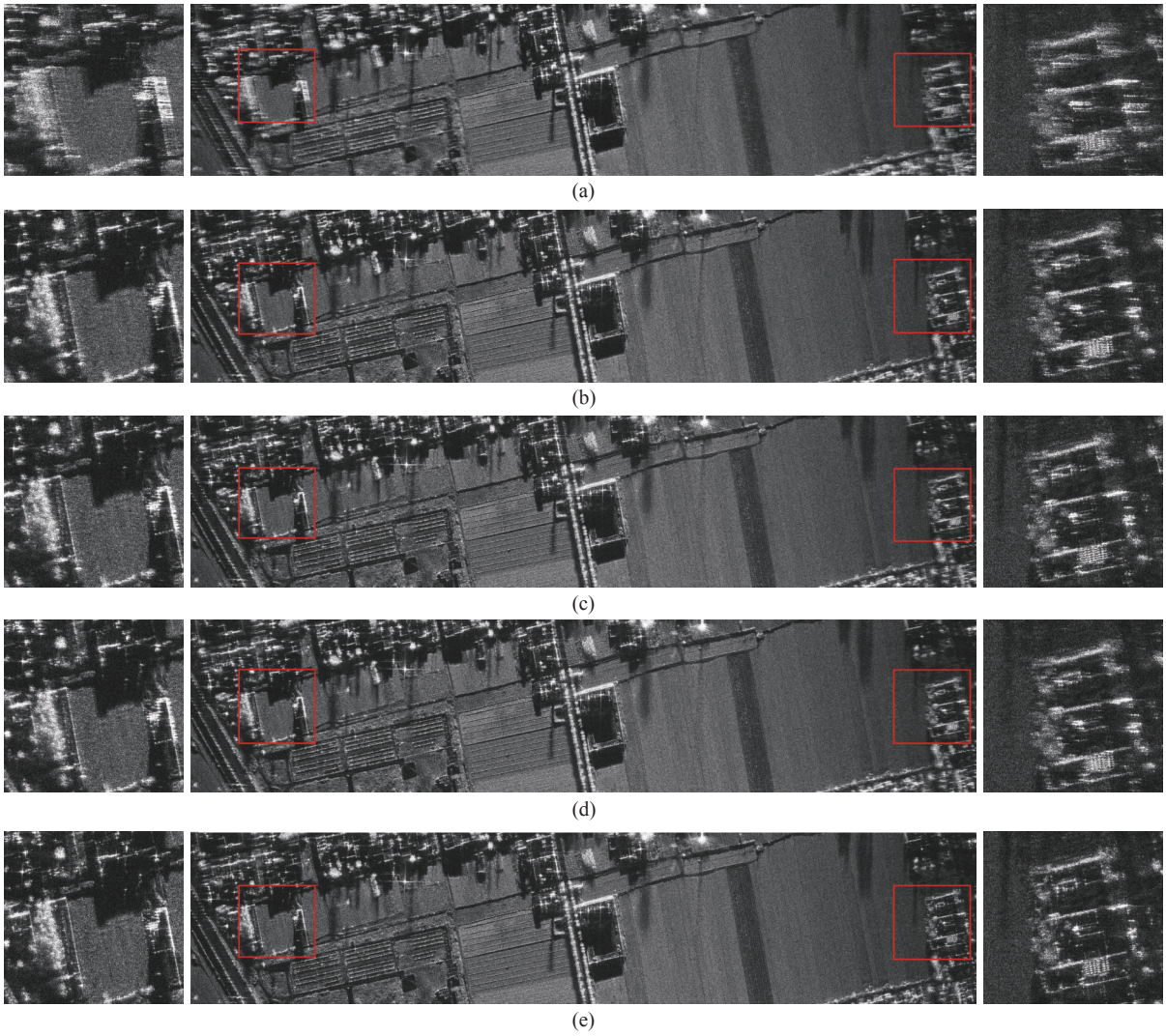

Fig. 10 Actual measurement data processing results by using: (a) traditional two-step algorithm; (b) 3-order NCS; (c) '3+4'-order NCS; (d) 2-order RS; (e) '2+3'-order RS

8 Conclusion

This paper summarizes and organizes the existing NL-SAR algorithms, mainly including variable standard algorithms, interpolation algorithms, hybrid algorithms, and time-domain algorithms. Simulation and actual data comparison were conducted for the most widely used variable standard algorithms and interpolation algorithms, and the imaging accuracy of the two types of algorithms is analyzed. The existing radar systems are increasingly developing towards multi-source, multi-dimensional, and multimodal directions. The existing NL-SAR imaging algorithms still face serious challenges. In the future, the development of NL-SAR imaging can consider multiple aspects such as high-efficiency time-domain imaging and new system imaging.

References:

[1] A. Moreira, P. Prats-Iraola, M. Younis, G. Krieger, I. Hajnsek, and K. P. Papathanassiou,"A tutorial on synthetic aperture radar," *IEEE Geoscience and Remote Sensing Magazine*, vol. 1, no. 1, pp. 6-43, 2013.

[2] J. Chen, M. Xing, H. Yu, B. Liang, J. Peng, and G. C. Sun,"Motion compensation/autofocus in airborne synthetic aperture radar: A review," *IEEE Geoscience and Remote Sensing Magazine*, vol. 10, no. 1, pp. 185-206, 2021.

[3] Y. Xiong, B. Liang, H. Yu, J. Chen, Y. Jin, and M. Xing,"Processing of bistatic SAR data with nonlinear trajectory using a controlled-SVD algorithm," *IEEE Journal of Selected Topics in Applied Earth Observations and Remote Sensing*, vol. 14, pp. 5750-5759, 2021.

[4] C. Hu, T. Long, Z. Liu, T. Zeng, and Y. Tian,"An improved frequency domain focusing method in geosynchronous SAR," *IEEE Transactions on Geoscience and Remote Sensing*, vol. 52, no. 9, pp. 5514-5528, 2013.

[5] Z. Ding, B. Shu, W. Yin, T. Zeng, and T. Long,"A modified frequency domain algorithm based on optimal azimuth quadratic factor compensation for geosynchronous SAR imaging," *IEEE Journal of Selected Topics in Applied Earth Observations and Remote Sensing*, vol. 9, no. 3, pp. 1119-1131, 2015.

[6] C. Hu, Z. Liu, and T. Long,"An improved CS algorithm based on the curved trajectory in geosynchronous SAR," *IEEE Journal of Selected Topics in Applied Earth Observations and Remote Sensing*, vol. 5, no. 3, pp. 795-808, 2012.

[7] J. C. Curlander,"Utilization of spaceborne SAR data for mapping," *IEEE Transactions on Geoscience and Remote Sensing*, vol. 2, pp. 106-112, 1984.

[8] P. Prats-Iraola, R. Scheiber, M. Rodriguez-Cassola, J. Mittermayer, S. Wollstadt, F. De Zan, B. Bräutigam, M. Schwerdt, A. Reigber, and A. Moreira,"On the processing of very high resolution spaceborne SAR data," *IEEE Transactions on Geoscience and Remote Sensing*, vol. 52, no. 10, pp. 6003-6016, 2014.

[9] K. Eldhuset,"Ultra high resolution spaceborne SAR processing," *IEEE Transactions on Aerospace and Electronic Systems*, vol. 40, no. 1, pp. 370-378, 2004.

[10] P. Wang, W. Liu, J. Chen, M. Niu, and W. Yang,"A high-order imaging algorithm for high-resolution spaceborne SAR based on a modified equivalent squint range model," *IEEE Transactions on Geoscience and Remote Sensing*, vol. 53, no. 3, pp. 1225-1235, 2014.

[11] B. Deng, X. Li, H. Wang, Y. Qin, and J. Wang,"Fast raw-signal simulation of extended scenes for missile-borne SAR with constant acceleration," *IEEE Geoscience and Remote Sensing Letters*, vol. 8, no. 1, pp. 44-48, 2010.

[12] S. Chen, H. Zhao, S. Zhang, and Y. Chen,"An extended nonlinear chirp scaling algorithm for missile borne SAR imaging," *Signal Processing*, vol. 99, pp. 58-68, 2014.

[13] J. Chen, M. Xing, G. C. Sun, and Z. Li,"A 2-D space-variant motion estimation and compensation method for ultrahigh-resolution airborne stepped-frequency SAR with long integration time," *IEEE Transactions on Geoscience and Remote Sensing*, vol. 55, no. 11, pp. 6390-6401, 2017.

[14] L. Zhang, Z. Qiao, M. D. Xing, L. Yang, and Z. Bao,"A robust motion compensation approach for UAV SAR imagery," *IEEE Transactions on Geoscience and Remote Sensing*, vol. 50, no. 8, pp. 3202-3218, 2012.

[15] X. H. Mao, H. Y. Cao, D. Y. Zhu, and Z. D. Zhu,"Prior knowledge aided two dimensional autofocus approach for synthetic aperture radar," *Acta Electonica Sinica*, vol. 41, no. 6, pp. 1041, 2013.

[16] J. Chen, G. C. Sun, M. Xing, J. Yang, Z. Li, and G. Jing,"A two-dimensional beam-steering method to simultaneously consider Doppler centroid and ground observation in GEO SAR," *IEEE Journal of Selected Topics in Applied Earth Observations and Remote Sensing*, vol. 10, no. 1, pp. 161-167, 2016.

[17] M. Bao, M. Xing, and Y. Li,"Chirp scaling algorithm for GEO SAR based on fourth-order range equation," *Electronics Letters*, vol. 48, no. 1, pp. 41-42, 2012.

[18] Y. Wu, G. C. Sun, C. Yang, J. Yang, M. Xing, and Z. Bao,"Processing of very high resolution spaceborne sliding spotlight sar data using velocity scaling," *IEEE Transactions on Geoscience and Remote Sensing*, vol. 54, no. 3, pp. 1505-1518, 2015.

[19] R. K. Raney, H. Runge, R. Bamler, I. G. Cumming, and F. H. Wong,"Precision SAR processing using chirp scaling," *IEEE Transactions on Geoscience and Remote Sensing*, vol. 32, no. 4, pp. 786-799, 1994.

[20] G. Davidson, I. G. Cumming, and M. Ito,"A chirp scaling approach for processing squint mode SAR data," *IEEE Transactions on Aerospace and Electronic Systems*, vol. 32, no. 1, pp. 121-133, 1996.

[21] S. Tang, "Study on imaging methods for SAR on curved-path platforms, " Ph.D. dissertation, Xidian University, 2017.

[22] C. Jianlai, X. Yi, X. Gang, Z. Junchao, Y. Degui, and L. Buge,"Nonlinear trajectory synthetic aperture radar imaging and autofocus algorithm based

on sub-image nonlinear chirp scaling," *Journal of Radars*, vol. 11, no. 6, pp. 1098-1109, 2022.

[23] L. Huang, X. Qiu, D. Hu, and C. Ding,"Focusing of medium-earth-orbit SAR with advanced nonlinear chirp scaling algorithm," *IEEE Transactions on Geoscience and Remote Sensing*, vol. 49, no. 1, pp. 500-508, 2010.

[24] Z. Li, M. Xing, Y. Liang, Y. Gao, J. Chen, Y. Huai, L. Zeng, G. C. Sun, and Z. Bao,"A frequency-domain imaging algorithm for highly squinted SAR mounted on maneuvering platforms with nonlinear trajectory," *IEEE Transactions on Geoscience and Remote Sensing*, vol. 54, no. 7, pp. 4023-4038, 2016.

[25] T. Zhang, Z. Ding, W. Tian, T. Zeng, and W. Yin,"A 2-D nonlinear chirp scaling algorithm for high squint GEO SAR imaging based on optimal azimuth polynomial compensation," *IEEE Journal of Selected Topics in Applied Earth Observations and Remote Sensing*, vol. 10, no. 12, pp. 5724-5735, 2017.

[26] A. Moreira and Y. Huang,"Airborne SAR processing of highly squinted data using a chirp scaling approach with integrated motion compensation," *IEEE Transactions on Geoscience and Remote Sensing*, vol. 32, no. 5, pp. 1029-1040, 1994.

[27] G. Sun, X. Jiang, M. Xing, Z. J. Qiao, Y. Wu, and Z. Bao,"Focus improvement of highly squinted data based on azimuth nonlinear scaling," *IEEE Transactions on Geoscience and Remote Sensing* , vol. 49 , no. 6, pp. 2308-2322, 2011.

[28] D. An, X. Huang, T. Jin, and Z. Zhou,"Extended nonlinear chirp scaling algorithm for high-resolution highly squint SAR data focusing," *IEEE Transactions on Geoscience and Remote Sensing*, vol. 50, no. 9, pp. 3595-3609, 2012.

[29] S. X. Zhang, M. D. Xing, X. G. Xia, L. Zhang, R. Guo, and Z. Bao,"Focus improvement of high-squint SAR based on azimuth dependence of quadratic range cell migration correction," *IEEE Geoscience and Remote Sensing Letters*, vol. 10, no. 1, pp. 150-154, 2013.

[30] J. Wu, Z. Li, Y. Huang, J. Yang, and Q. H. Liu,"A generalized omega-k algorithm to process translationally variant bistatic-SAR data based on two-dimensional stolt mapping," *IEEE Transactions on Geoscience and Remote Sensing*, vol. 52, no. 10, pp. 6597-6614, 2014.

[31] D. D'Aria and A. M. Guarnieri,"High-resolution spaceborne SAR focusing by SVD-stolt," *IEEE Geoscience and Remote Sensing Letters*, vol. 4, no. 4, pp. 639-643, 2007.

[32] J. Chen, G. C. Sun, M. Xing, B. Liang, and Y. Gao,"Focusing improvement of curved trajectory spaceborne SAR based on optimal LRWC preprocessing and 2-D singular value decomposition," *IEEE Transactions on Geoscience and Remote Sensing*, vol. 57, no. 7, pp. 4246-4258, 2019.

[33] J. Chen, J. Zhang, Y. Jin, H. Yu, B. Liang, and D. G. Yang,"Real-time processing of spaceborne SAR data with nonlinear trajectory based on variable PRF," *IEEE Transactions on Geoscience and Remote Sensing*, vol. 60, pp. 1-12, 2021.

[34] W. Liu, G. Jing, G. Sun, Q. Chen, and M. Xing,"Medium-earth-orbit SAR data focusing method based on two-step azimuth resampling," *Journal of Electronics and Information Technology*, vol. 41, no. 1, pp. 136-142, 2019.

[35] J. Ding, Y. Li, M. Li, and J. Wang,"Focusing high maneuvering bistatic forward-looking SAR with stationary transmitter using extended keystone transform and modified frequency nonlinear chirp scaling," *IEEE Journal of Selected Topics in Applied Earth Observations and Remote Sensing*, vol. 15, pp. 2476-2492, 2022.

[36] W. Liu, G. C. Sun, M. Xing, H. Li, and Z. Bao,"Focusing of MEO SAR data based on principle of optimal imaging coordinate system," *IEEE Transactions on Geoscience and Remote Sensing*, vol. 58, no. 8, pp. 5477-5489, 2020.

[37] M. Albuquerque, P. Prats, and R. Scheiber, "Applications of time-domain back-projection SAR processing in the airborne case, " in *7th European Conference on Synthetic Aperture Radar*, pp. 1-4, 2008.

[38] A. F. Yegulalp, "Fast backprojection algorithm for synthetic aperture radar, " in *Proceedings of the 1999 IEEE Radar Conference. Radar into the Next Millennium (Cat. No. 99CH36249)*, pp. 60-65, 1999.

[39] J. Chen and H. Yu,"Wide-beam SAR autofocus based on blind resampling," *Science China Information Sciences*, vol. 66, no. 4, pp. 140304, 2023.

[40] L. Zhang, H. L. Li, Z. J. Qiao, and Z. W. Xu,"A fast BP algorithm with wavenumber spectrum fusion for high-resolution spotlight SAR imaging," *IEEE Geoscience and Remote Sensing Letters*, vol. 11, no. 9, pp. 1460-1464, 2014.

[41] Q. Dong, G. C. Sun, Z. Yang, L. Guo, and M Xing,"Cartesian factorized backprojection algorithm for high-resolution spotlight SAR imaging," *IEEE Sensors Journal*, vol. 18, no. 3, pp. 1160-1168, 2018.

[42] Y. Luo, F. Zhao, N. Li, and H. Zhang,"An autofocus cartesian factorized backprojection algorithm for spotlight synthetic aperture radar imaging," *IEEE Geoscience and Remote Sensing Letters*, vol. 15, no. 8, pp. 1244-1248, 2018.

Yi Xiong is currently working toward the Ph.D. degree with Central South University. His research interests include bistatic SAR imaging and nonlinear trajectory SAR imaging.

Buge Liang received the B.S. and Ph.D. degrees from the National University of Defense Technology (NUDT), Changsha, China, in 2001 and 2007, respectively. He is a Full Professor with Central South University (CSU), Changsha. His research interests include electromagnetic measurement technologies, high-power nanosecond pulsers, and ultrawideband (UWB) radar.

Ning Wang is mainly engaged in the overall design of radar systems and the identification of space debris characteristics, including microwave imaging of space targets, ISAR image processing, 2D image feature recognition, attitude estimation based on key components of 2D images, 3D reconstruction, etc. As the project leader and technical leader, he has undertaken multiple pre research projects or received multiple provincial and ministerial level awards.

Jianlai Chen received the B.S. degree in electronic engineering and the Ph.D. degree in signal and information processing from Xidian University, Xi'an, China, in 2013 and 2018, respectively. He is currently an Associate Professor with Central South University (CSU), Changsha, China. He has authored or coauthored one book and more than 20 research articles in high-impact peer-reviewed journals. His research interests include synthetic aperture radar (SAR) imaging, SAR motion compensation (MoCo) and autofocus, and machine learning.